

Variation of Leading-Edge Suction at Stall for Steady and Unsteady Airfoil Motions

Shreyas Narsipur,* Pranav Hosangadi,† Ashok Gopalarathnam,‡ and Jack R. Edwards§

*Department of Mechanical and Aerospace Engineering,
North Carolina State University, Raleigh, NC 27695-7910*

Computational results for steady and unsteady airfoil motions are used to study the variation of leading-edge suction at stall. Computations were performed on the NACA0012 symmetric airfoil and the SD7003 cambered airfoil using an unsteady RANS code that was validated against steady and unsteady experimental results. A parametric study was performed to determine the behavior of leading-edge suction with variations in pitch rate and Reynolds numbers. Results showed that flowfield structures of unsteady low pitch rate motions were similar to steady results for a given amount of trailing-edge separation. The overshoot in lift and suction coefficient can be attributed to the boundary layer convection lag. For LEV dominated flows, it is found that flow morphology after LEV initiation is similar regardless of motion parameters. However, the time instance and flowfield structure at the point of LEV initiation varied for low and high Reynolds numbers. While LESP values at LEV initiation for low Reynolds number simulations were found to be independent of motion kinematics, the same was not true for the high Reynolds number cases.

Nomenclature

A_0	leading-edge Fourier term coefficient
c	airfoil chord
C_l	airfoil lift coefficient
C_{lmax}	airfoil maximum lift coefficient
C_p	coefficient of pressure, $\frac{p-p_\infty}{q_\infty}$
C_s	airfoil suction force coefficient
C_{smax}	airfoil maximum suction coefficient
f	separation point location as % of chord
$\vec{\delta}_l$	panel vector
\vec{F}'_{LE}	leading-edge force per unit span
\vec{F}'_s	leading-edge suction force per unit span
K	non-dimensional pitch rate, $\frac{\dot{\alpha}c}{2U_\infty}$
k	reduced frequency, $\frac{\omega c}{2U_\infty}$
$LES\,P$	leading-edge suction parameter
q_∞	dynamic pressure, $\frac{1}{2}\rho U_\infty^2$
Re	Reynolds number
U_∞	freestream velocity

*Graduate Research Assistant, shreya@ncsu.edu. Student Member AIAA

†Graduate Research Assistant, phosang@ncsu.edu. Student Member AIAA

‡Associate Professor, ashok_g@ncsu.edu, (919) 515-5669. Associate Fellow AIAA

§Professor, jredward@ncsu.edu, (919) 515-5264. Associate Fellow AIAA

I. Introduction

Unsteady aerodynamics research has gained significant popularity in the aerodynamic community due to its applications in a wide range of areas that include, but not limited to, dynamic stall in helicopters and wind turbines [1, 2], bio-inspired flight [3], micro air vehicle (MAV) design [4], leading-edge vortices in delta-wings [5], and flow-energy harvesting devices [6]. A crucial area of research in unsteady aerodynamics is understanding the flow physics of time-dependent separation and stall, and its variations based on airfoil shape, Reynolds number, and motion kinematics. While theoretical work in unsteady aerodynamics, primarily by Theodorsen [7] and Wagner [8], dates back to 1920s and 1930s, the late 1960s saw a renewed interest in unsteady fluid flows due to the dynamic stall problem in helicopters [9]. Though analytical studies by Carta [10, 11] and Ericsson and Reding [12] helped understand and predict dynamic stall, the methods were restricted to low pitch rate motions and the availability of static experimental data. Extensive experimental studies by McCroskey et al. [13], McAlister et al. [14], Carr et al. [15], and McAlister and Carr [16] provided a major leap in understanding and predicting dynamic stall. McCroskey [17, 18] characterized the phenomenon of dynamic stall by a delay in the onset of flow separation and the shedding of concentrated vorticity, popularly known as dynamic stall vortex (DSV) or leading-edge vortex (LEV), from the leading-edge of the airfoil. McCroskey et al.'s [19–21] three part review on experimental studies of dynamic stall showed that while pitch rate and airfoil shape, specifically the leading-edge profile, had major effects on the aerodynamic loads and strength of the LEV, the Reynolds number effects were small.

Improvements in supercomputing capabilities allowed for various aspects of dynamic stall to be studied extensively [22–29]. Recent research interests in insect/bird flight and MAV aerodynamics have pushed the boundaries of unsteady aerodynamics to include time-dependent motions at lower Reynolds numbers and higher pitch rates and has spurred many computational and experimental studies on the subject [30–33]. All the while, theoretical models have been developed and improved based on the findings of experimental and computational studies [34–41] for use in rapid design and analysis activities.

The onset of separation and formation of the LEV is governed by criticality of flow parameters at the leading-edge. Experiments and computational studies by Evans and Mort [42], Beddoes [43], Jones and Platzer [44], Chandrasekhara et al. [45], and Ekaterinaris and Platzer [46] have provided conclusive evidence which suggests that a pressure-lag on the airfoil surface delays the occurrence of leading-edge flow separation for all pitch rates. Jones and Platzer [47] further concluded that the onset of the LEV occurs for a critical pressure distribution that is independent of motion kinematics. As proposed by Katz [37], real airfoils have rounded leading-edge which can support some suction even when flow at the leading-edge is separated. The amount of suction that can be supported is a characteristic of the airfoil shape and Reynolds number. Recent research by Ramesh et al. [48, 49] shows that an inviscid parameter, termed the leading-edge suction parameter (LESP), that is set to the A_0 coefficient of the Fourier series solution at any given time step, is a measure of suction at the leading-edge. The instantaneous LESP value exceeding the critical LESP value marks the initiation of LEV formation. The LESP was found to be independent of motion kinematic parameters such as amplitude, pitch rate, and pivot location, thereby making it a logical choice for representation of flow criticality at the leading-edge. The LESP concept has been implemented in a low-order method called LDVM which was developed for rapid prediction of low-Mach number flows over unsteady airfoil motions with intermittent LEV shedding.

The aim of the current work is to computationally study steady and unsteady airfoil motions for two airfoils: the NACA0012 symmetric airfoil and the SD7003 cambered airfoil. The focus will be to study the variation in flow-field structures and leading-edge suction with airfoil shape, Reynolds number, and motion kinematics. Drawing inspiration from the success of the LDVM, efforts have been made to determine the magnitude of leading-edge suction from computational pressure measurements and relating the suction data to the LESP. The results from the current work aims at aiding on-going research efforts by the authors [50] in developing an augmented theoretical method for rapid prediction of dynamic stall.

The following section (Section II) discusses the computational methodology along with the validation of the numerical scheme with experimental data. Section II also provides a method for extracting the leading-edge suction force from the numerical results and relating the suction coefficient (C_s) to the LESP. Computational results for steady and unsteady motions are presented in Section III and a parametric study of the variation in the LESP is conducted for varying pitch rate and Reynolds number. The final section (Section IV) lists the conclusions drawn from the current research.

II. Methodology

In this section, a brief description of the unsteady RANS CFD code used in this work is presented in subsection A followed by the validation of the numerical scheme with existing experimental data in subsection B. The subsequent subsection C provides details regarding the calculation of the suction force from computational pressure data and

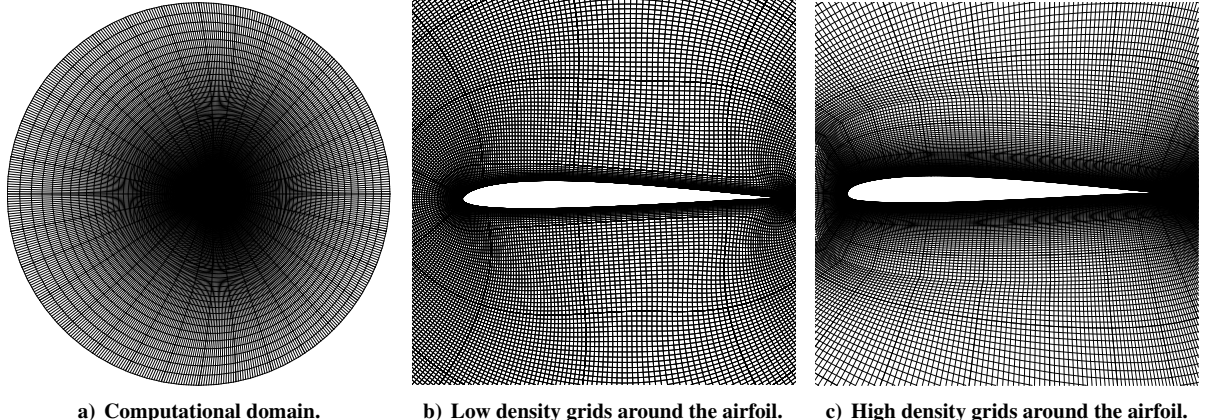


Figure 1: Computational grids for the SD7003 airfoil used in computations.

relating the suction coefficient to the LESP.

A. CFD Method

CFD calculations were performed using NCSU's REACTMB-INS code, which solves the time-dependent incompressible Navier-Stokes equations using a finite-volume method. The governing equations are written in arbitrary Lagrangian / Eulerian (ALE) form, which enables the motion of a body-fitted computational mesh in accord with prescribed rate laws. Spatial discretization of the inviscid fluxes uses a low-diffusion flux-splitting method valid in the incompressible limit [51]. This method is extended to higher-order spatial accuracy using Piecewise Parabolic Method interpolations of the primitive variables $[p, u, v, w]^T$ and transported variable for the S-A model, \tilde{v} . Viscous terms are discretized using second-order central differences. A dual-time stepping method is used to integrate the equations in time. An artificial compressibility technique, discretized in a fully implicit fashion and solved approximately using ILU decomposition, is used to advance the solution in pseudo-time. Typically, eight sub-iterations per physical time step were needed to reduce the residual errors two orders of magnitude. The Spalart-Allmaras model [52] as implemented by Edwards and Chandra [53], is used for turbulence closure. Three 2-D body-fitted grids were generated: one low density grid for low Reynolds number simulations of the SD7003 containing 50,622 cells and two high density grids for high Reynolds number simulations of the NACA0012 and SD7003 containing 140,400 and 92,400 cells respectively. Computational grids for the SD7003 airfoil are shown in Fig. 1.

B. CFD Validation

Two test computations were performed to establish the accuracy of the numerical code. Steady simulations were performed for the NACA0012 at a freestream Reynolds number of 2.5 million and the computed C_l was compared with experimental data from Carr et al. [15]. Observations from Fig. 2 show that computed C_l is within 5% of experimental data for all angles of attack. Next, an unsteady simulation was performed for the SD7003 airfoil at a freestream Reynolds number of 30,000 and non-dimensional pitch rate (K) of 0.11 for a pitch up-hold-return motion defined using the Eldredge function [31, 54]. Figure 3 compares computed C_l data with experimental data obtained from US Air Force Research Laboratory's (AFRL) Horizontal Free-surface Water Tunnel [49]. The computed C_l agrees well with experiment in the pitch-up region but is slightly over-predicted in the hold and return regions of the motion. Computations also correctly capture the locations and intensities of the spikes due to apparent-mass effects.

C. Determination of Suction Force

The net force acting on an airfoil can be resolved into two components – a chordwise force acting along the chord and a normal force acting perpendicular to the chord. The chordwise force is often a “suction” force acting in the direction opposite to the trailing-edge and appears to pull the airfoil forward.

When the stagnation point is not at the leading-edge, the flow is forced to travel back towards and around the leading-edge. The curvature of flow gives rise to a low-pressure region near the leading-edge called the suction peak.

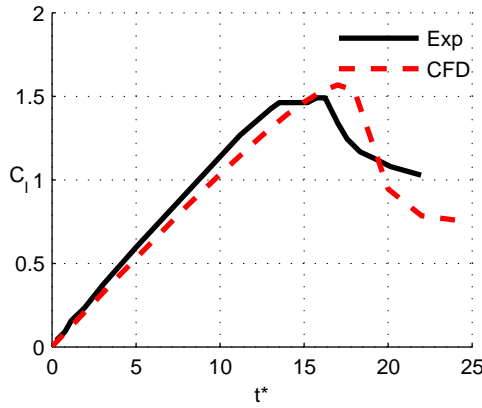


Figure 2: Comparison of steady experimental [15] and computed C_l for NACA0012 at $Re = 2.5 \times 10^6$.

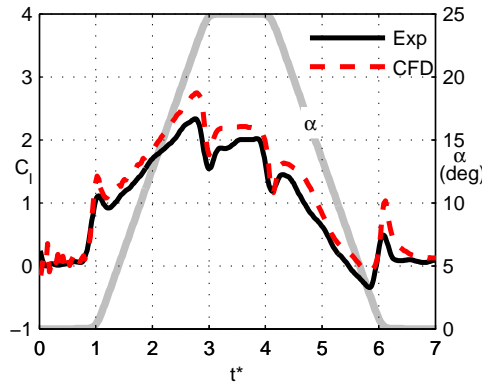


Figure 3: Comparison of experimental [49] and computed C_l for SD7003 at $Re = 30,000$, $K = 0.11$, $\alpha_{max} = 25^\circ$.

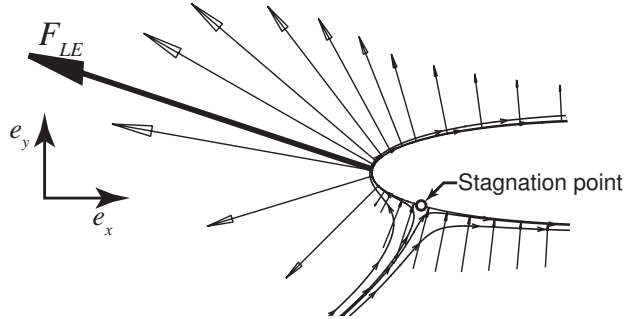


Figure 4: Representation of the leading-edge force vector.

The net force on this region, as seen in Fig. 4, is the leading-edge force which when resolved in the chordwise direction is the suction force.

The suction force on the airfoil is calculated from CFD by integrating the pressure force on panels within a predefined maximum distance from the leading-edge. The net force at the leading-edge and the suction force are calculated as,

$$\vec{F}'_{LE} = q_\infty \sum_{x/c=0}^{x_{max}/c} [C_p (\vec{\delta}_l \times \vec{e}_z)] \quad (1)$$

$$\vec{F}'_s = (\vec{F}'_{LE} \cdot \vec{e}_x) \vec{e}_x \quad (2)$$

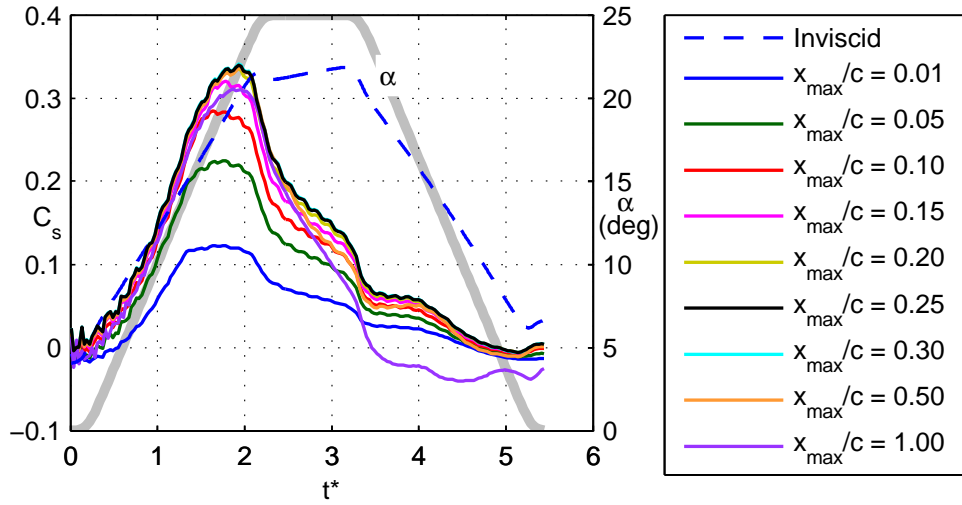


Figure 5: Change in C_s caused by variation of the x_{max}/c of integration.

where, q_∞ is the dynamic pressure, $\vec{\delta}_l$ is the vector connecting the two end-points of the panel, and \vec{e}_x and \vec{e}_z are the unit vectors in the X and Z directions respectively. The limit upto which panels are included in the suction force calculation is given by x_{max}/c .

As seen in Fig. 5, it was observed that beyond x_{max}/c of 25%, the suction force was relatively independent of the selected x_{max}/c for a pitch up-hold-return motion with $K = 0.11$ for the SD7003 pivoted at the leading-edge and simulated at a Reynolds number of 30,000. Thus, the suction force in this work was defined as the chordwise component of the net pressure force acting on the forward 25% of the airfoil. The suction force, non-dimensionalized by the dynamic pressure and chord, gives the suction force coefficient C_s .

$$C_s = \frac{|\vec{F}'_s|}{q_\infty c} \quad (3)$$

Studies by Ramesh et al. [48] showed that suction force coefficient is proportional to the square of the LESP and is formulated as,

$$C_s = 2\pi(LES P)^2 \quad (4)$$

III. Results

Computations were performed for two airfoils and the results presented are divided into three case studies. Subsection A presents steady results for the NACA0012 airfoil at a freestream Reynolds number of 3.0 million. Unsteady results for the NACA0012 at a freestream Reynolds number of 3.0 million for non-dimensional pitch rates ranging from 0.0025 to 0.25 are presented in subsection B with detailed analysis of the effect pitch rate has on the flow-field structures and aerodynamic loads, particularly the suction force. Subsection C presents unsteady results for the SD7003 airfoil for non-dimensional pitch rates between 0.10 to 0.60 at two freestream Reynolds numbers (30,000 and 3,000,000) in order to analyze the effect of Reynolds number variation on flowfield structures and suction force. All unsteady motions presented have been defined using the Eldredge function [31, 54] with the airfoils being pivoted at either the leading-edge or quarter-chord.

A. Steady Simulations

Figure 6 shows the contour plots of vorticity and velocity magnitude for the steady simulations of the NACA0012 airfoil at a freestream Reynolds number of 3.0 million. Also plotted on the contours are the flow stagnation, separation, and reattachment points on the airfoil surface. We observe that when the separation location (f) is at 75% of the chord (Figs. 6(a) & 6(e)), the region of reversed flow is small and lift, suction, drag, and moment continues to increase (Fig. 7). As separation location progresses to 50% of the chord, the flow reversal region increases (Figs. 6(b) & 6(f)) causing a drop in lift, suction, and moment and increase in drag (Fig. 7). With further increase in angle of attack, separation point continues to move towards the leading-edge all the while causing an increase in area of the separation region (Figs. 6(c) & 6(g)). Finally, when the separation region is at the leading-edge, flow reversal is seen over the

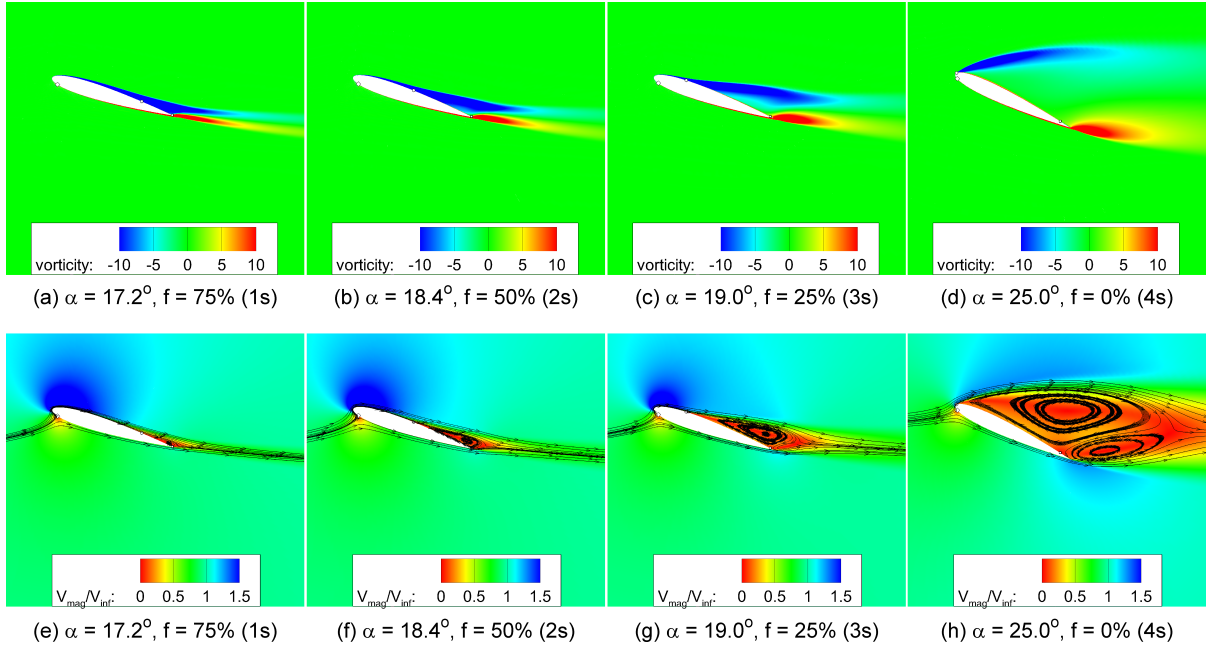


Figure 6: Vorticity (a – d) and velocity magnitude (e – h) contours for NACA0012 steady simulations ($Re = 3 \times 10^6$).

entire suction surface of the airfoil, as seen in Figs. 6(d) & 6(h). At this point, while there is a sharp drop in moment and sudden increase in drag, lift and suction are low and remain relatively constant with increasing angle of attack (Fig. 7).

B. Effect of Pitch Rate Variation

Unsteady pitch up-return motions were simulated for non-dimensional pitch rates ranging from $K = 0.0025$ to $K = 0.25$ for the NACA0012 airfoil at a freestream Reynolds number of 3.0 million to study the effects of pitch rate variation on general flowfield and aerodynamic load characteristics. The pitch rate was divided into three regions depending on the magnitude of trailing-edge separation during airfoil pitch up: low- K ($0 \leq K \leq 0.01$), medium- K ($0.01 < K \leq 0.075$), and high- K ($K > 0.075$). Figures 8, 9, and 10 show the vorticity and velocity magnitude plots for the low- K ($K = 0.005$, 0° - 35° - 0° pitch up-return), medium- K ($K = 0.05$, 0° - 45° - 0° pitch up-return), and high- K ($K = 0.25$, 0° - 90° - 0° pitch up-return) cases respectively.

When undergoing pitch-up motion from a low angle of attack, the flow on the upper surface of the airfoil typically remains fully attached and lift continues to increase even as the angle of attack exceeds that for steady stall as seen in Fig. 7(d). This behavior is often called “lift overshoot.” Subsequent events depend on the value of the non-dimensional pitch rate for ramp motions (or on the reduced frequency k for sinusoidal motions). If the airfoil continues to pitch up and the K is large, high suction and associated adverse pressure gradient at the leading-edge results in the formation of an LEV (Fig. 10). The initiation of LEV formation, its growth, termination/pinch-off from the leading edge, convection down the upper surface and off the chord of the airfoil are subsequent events that determine the time variations of forces and moments on the airfoil. On the other hand, for very low- K , of which steady flow with $K = 0$ is a subset, the boundary layer flowing from the leading edge to trailing edge of the upper surface experiences adverse gradient. At some high pitch angle the adverse gradient causes the boundary layer to separate, resulting in trailing-edge stall without being accompanied by the formation of an LEV (Fig. 8). In many situations, in which the K is moderate, dynamic stall could occur due to a combination of trailing-edge stall along with LEV formation (Fig. 9). For better clarity, we will consider the low- K (non-LEV) and medium/high- K (LEV dominated) flows separately during the discussion.

Comparing the contour plots of the low K simulations in Fig. 8 with the steady contours in Fig. 6 shows that the general flowfield structures for a given separation location is similar. Figure 7 further shows that the aerodynamic loads of the low- K motion follow a similar trend when compared to steady data during the up-stroke with the exception of the lift overshoot phenomenon. The lift overshoot is often attributed to one or more time lags in the aerodynamics, particularly the boundary layer convection lag. The boundary layer convection lag, discussed by Ericsson and Red-

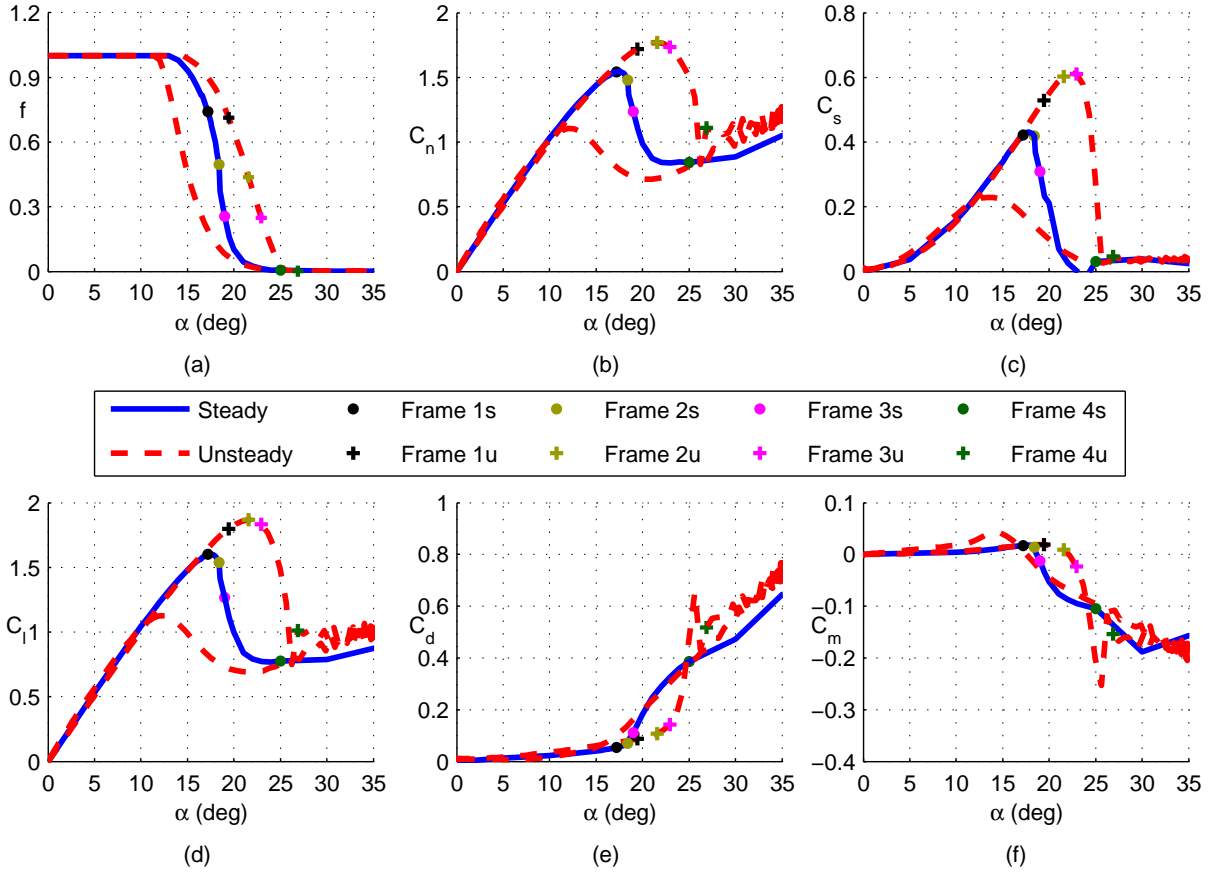


Figure 7: Comparison of steady and low- K ($K = 0.005$) coefficient data. Frames 1s – 4s correspond to Fig. 6 and frames 1u – 4u correspond to Fig. 8.

ing [55], is the lag in the net adverse pressure gradient experienced by the boundary layer in unsteady flow. The idea is that, in the time that the boundary layer takes to travel from the leading edge to the trailing edge, the airfoil has pitched up to a higher angle. Thus the pressure gradient that the boundary layer experiences is not the instantaneous pressure gradient, but a quasi-steady pressure gradient. Further details regarding the aerodynamic time lag can be found in Ref. 50. Overall, the delay in stall effectively increases the maximum lift and suction coefficients and delays moment stall. We also see from Fig. 7 that C_{lmax} does not correspond to C_{smax} in the unsteady case. However, in deep stall (Figs. 8(d) & 8(h)), the unsteady low- K aerodynamic coefficients are approximately equal to steady coefficients.

Observation of the contour plots in Figs. 9 and 10 show that the flow morphology after the initiation of the LEV for both the medium and high- K cases are similar. However, differences are seen in the boundary layer before the formation of the LEV. In the medium- K case, the boundary layer is much thicker (Figs. 9(a) & 9(e)) as compared to the high- K case (Figs. 10(a) & 10(e)). The difference in boundary layer thickness can be attributed to the fact that trailing-edge separation has progressed up to 40% of the chord in the medium- K case causing a larger reversed flow region on the suction surface beyond the separation point as compared to the high- K case where trailing-edge separation is within 95% of the chord. Also, the angle of attack at which LEV initiation occurs for the high- K case is higher than that of the medium- K case due to a higher boundary-layer convection lag for the faster pitch rate case. As mentioned earlier, the events that occur during and after the formation of the LEV are consistent. In the current work, three critical events of interest are chosen and the variation of the flow and degree of leading-edge suction (represented here by the LESP) for each of these events are analyzed.

Event 1 shown in Fig 11(b), is the time step at which C_f close to the leading-edge (within 10% of the chord) becomes negative. The second event (event 2), illustrated in Fig. 12(a), is the time step at which LESP is maximum. The third and final event of interest (event 3) is the appearance of a secondary recirculating region, opposite in direction to the first LEV, near the leading-edge, as shown in Fig 13.

On identifying the points of interest, LESP data for all medium and high- K simulations was calculated and plotted in Fig 14 for the three events. We observe that the LESP for events 2 and 3 increases with increase in pitch rate.

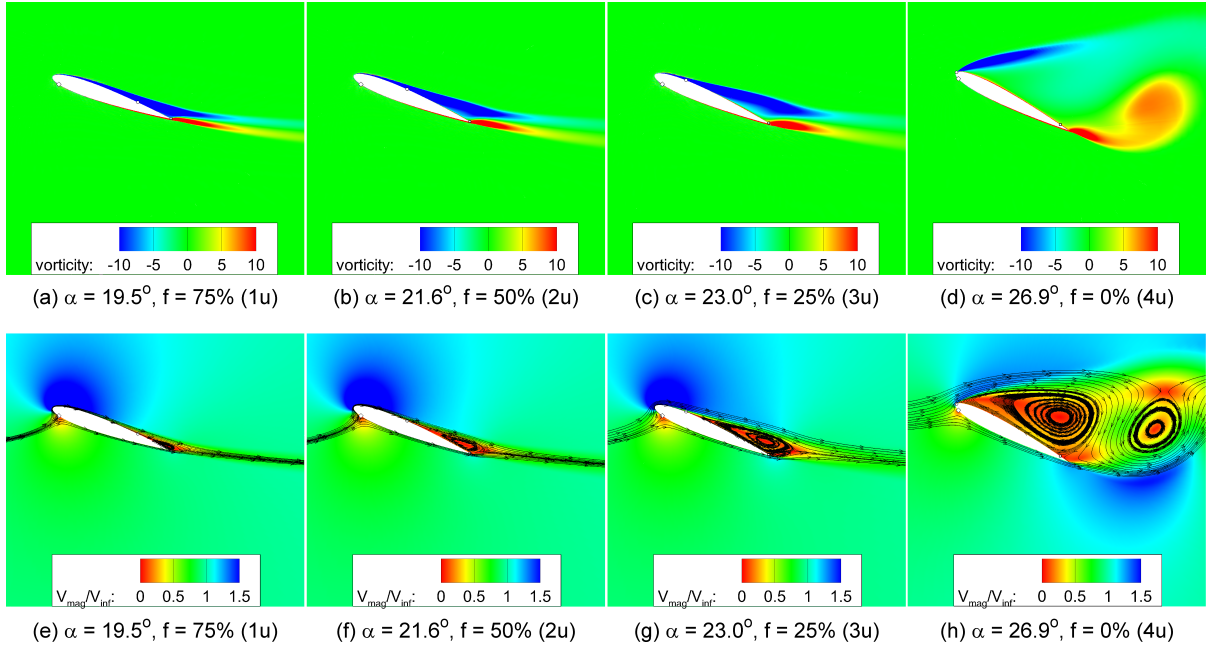


Figure 8: Vorticity (a – d) and velocity magnitude (e – h) contours for NACA0012 unsteady simulations ($Re = 3 \times 10^6$, $K = 0.005$, 0° - 35° - 0° pitch up-return).

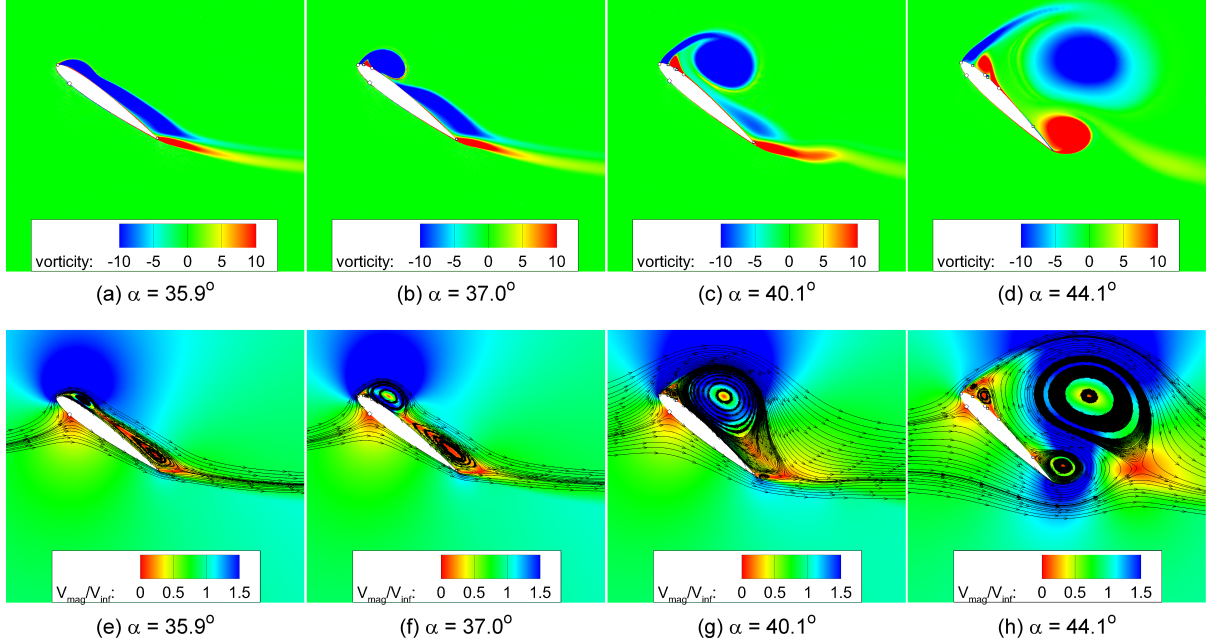


Figure 9: Vorticity (a – d) and velocity magnitude (e – h) contours for NACA0012 unsteady simulations ($Re = 3 \times 10^6$, $K = 0.05$, 0° - 45° - 0° pitch up-return).

There is also significant variation in the LESP at events 2 and 3 for varying pivot locations. However, the LESP for event 1 is relatively independent of the pitch rate and pivot location. The large spread of LESP values is inconsistent with the findings of Ramesh et al. [49], who showed the LESP at event 3 to be independent of motion kinematics. A probable cause could be that the operating freestream Reynolds number in the current work is higher than that presented in Ref. 49 where the range of Reynolds numbers simulated are between 1,000 to 100,000. The effect of Reynolds number on the LESP, particularly at the three events of interest, is investigated in subsection C.

Another interesting observation that can be made from Figs. 11 – 13 is that though negative C_f and therefore

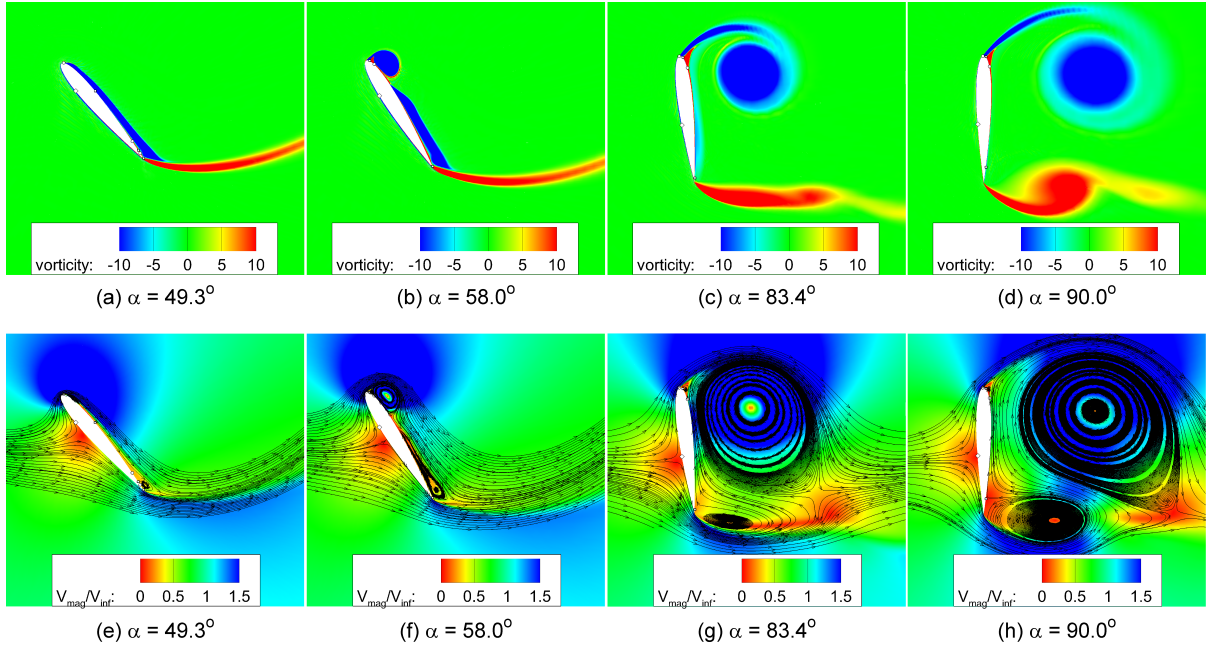


Figure 10: Vorticity (a – d) and velocity magnitude (e – h) contours for NACA0012 unsteady simulations ($Re = 3 \times 10^6$, $K = 0.25$, 0° - 90° - 0° pitch up-return).

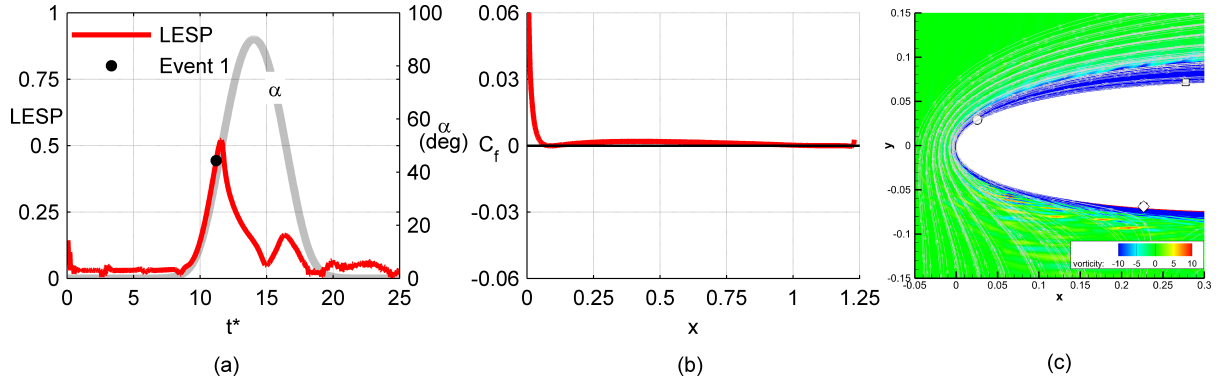


Figure 11: Event 1.

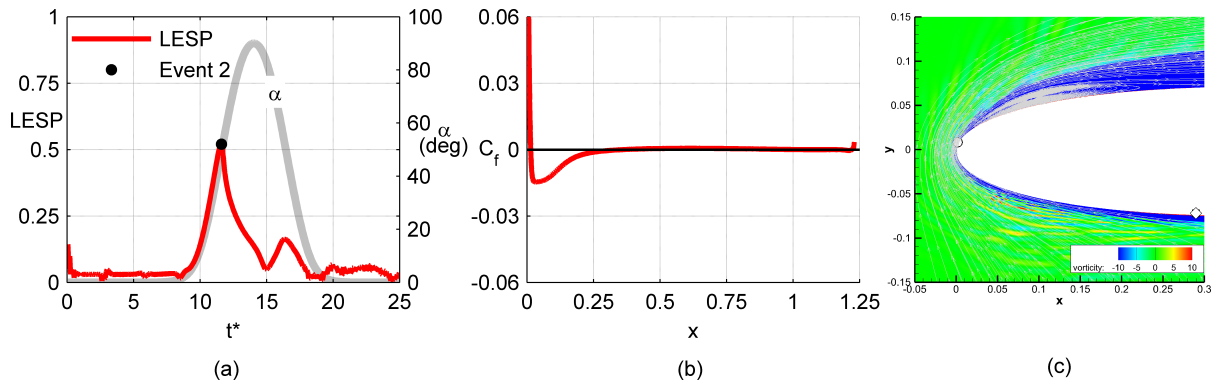


Figure 12: Event 2.

the signature of the separation bubble occurs at event 1, LEV initiation does not start until event 2. By the time a

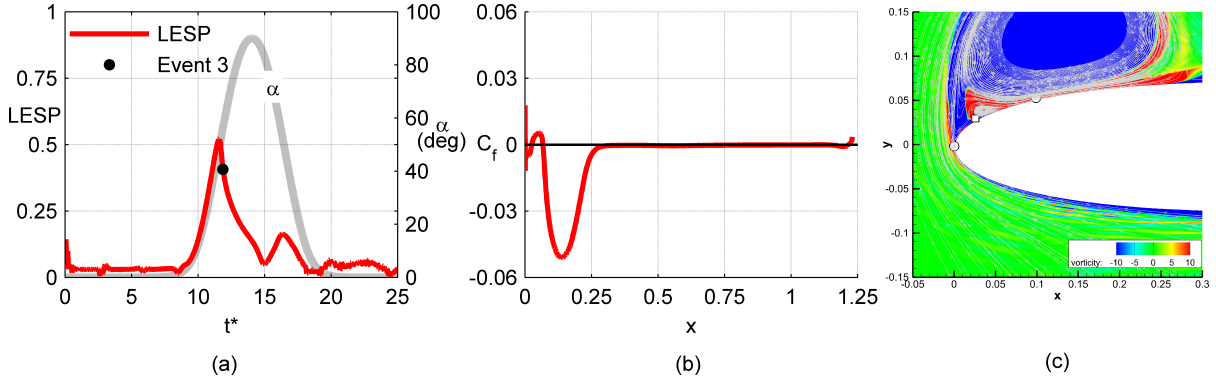


Figure 13: Event 3.

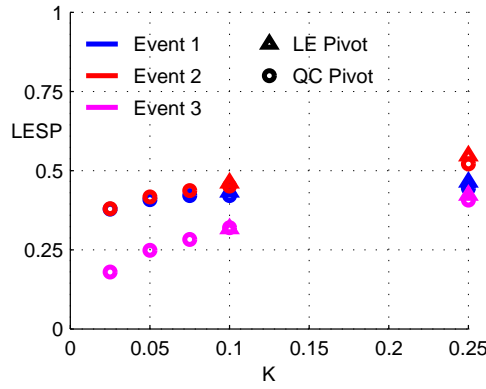


Figure 14: Variation of LESP with K for the three critical events.

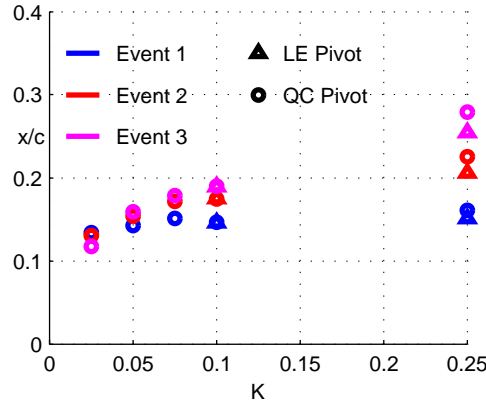


Figure 15: Variation of stagnation point with K for the three critical events.

secondary recirculating region appears in the vicinity of the leading-edge (event 3), the primary LEV has lifted-off from the airfoil surface.

Figure 15 plots the variation of the stagnation point location with varying pitch rate and pivot locations for the three events. The observed trends in stagnation point variation are similar to that of the LESP: event 1 is independent of motion kinematics while the stagnation points for events 2 and 3 progress farther away from the leading-edge with increasing pitch rate.

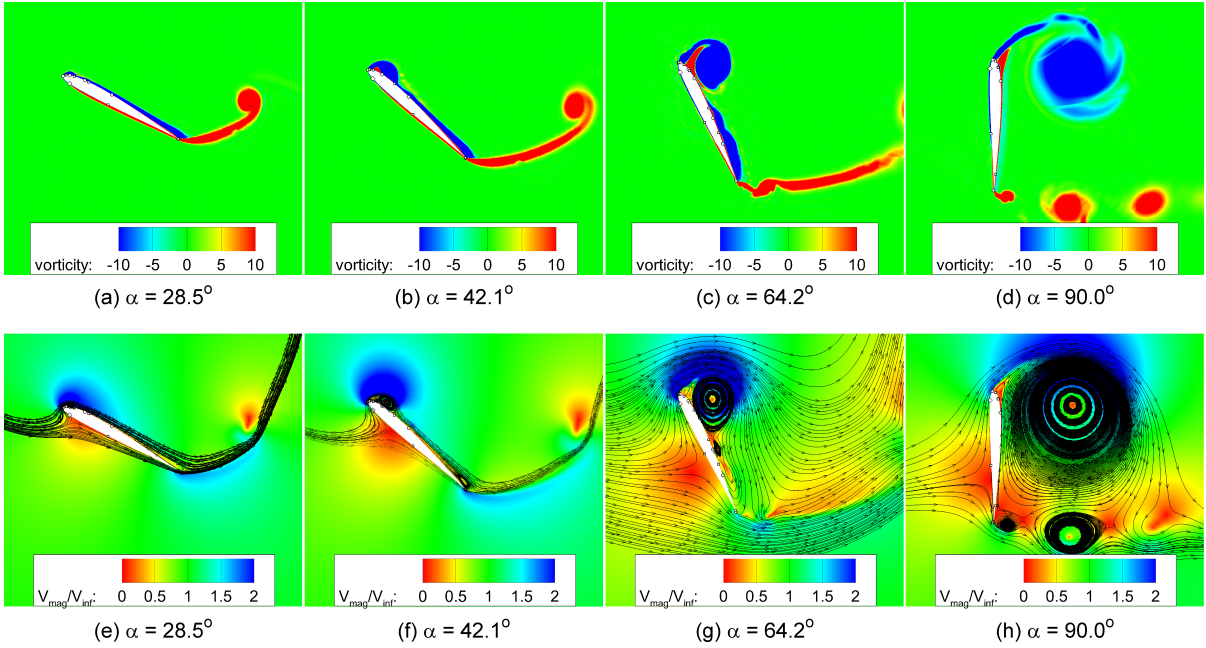


Figure 16: Vorticity (a – d) and velocity magnitude (e – h) contours for SD7003 unsteady simulations ($Re = 3 \times 10^4$, $K = 0.40$, 0° - 90° - 90° - 0° pitch up-hold-return).

C. Effect of Reynolds Number Variation

The SD7003 airfoil was simulated for low (30,000) and high (3,000,000) Reynolds numbers for high non-dimensional pitch rates between 0.10 and 0.60. The objective of these simulations was to determine the differences in flowfield structures and suction force at the two Reynolds numbers. The motion considered for comparison was a pitch up-hold-return motion with the airfoil pivoted at the quarter-chord. Figures 16 and 17 show the flowfield contours for the low and high Reynolds number simulations respectively, from the point of LEV initiation. The first difference between the two cases, as seen on comparing Figs. 16(a,e) & 17(a,e), is that the boundary layer over the suction surface aft of the trailing-edge is thicker for the low Reynolds number case as the trailing-edge separation has progressed up to 55% of the chord while it is beyond 95% of the chord for the high Reynolds number case. Secondly, the angle of attack at which LEV initiation occurs is greater for the high Reynolds number case as compared to the low Reynolds number case. Flow contours after initiation of LEV (Figs 16(b – d, f – h) & Figs 17(b – d, f – h)) follow similar trends for both low and high Reynolds number cases.

In order to study the variation in suction force, we look at the LESP data at the three events plotted in Figs. 18 to 20 and analyze the corresponding flow contours at the leading-edge for the event under consideration. For event 1, it can be observed from Figs. 18(b) and 18(d) that the streamlines for both the low and high Reynolds number simulations follow similar trends. Significant differences are found at event 2 (Figs. 19(b) and 19(d)) where the low Reynolds number streamline contour shows an LEV that is almost off the surface with a secondary recirculating zone starting to form close to the leading-edge while the LEV has just begun to form for the high Reynolds number case. Event 3 vorticity contours (Figs. 20(b) and 20(d)) show that the LEV has just started to initiate for the low Reynolds number case while the LEV is lifting off the surface with a secondary recirculating region at the leading-edge for the high Reynolds number case.

On comparing the LESP plots for all three cases (Figs. 18(a,c) , 19(a,c), and 20(a,c)), we see that while event 1 occurs first for both Reynolds number solutions, event 3 precedes event 2 for the low Reynolds number case while the opposite is true for the higher Reynolds number case. Also, while event 2 can be taken as the point of LEV initiation for the high Reynolds number simulation, event 3 is a better signature for LEV initiation in the low Reynolds number case as the LEV has fully formed by event 2.

Figures 21 and 22 show the LESP variation with pitch rate and pivot location at the three critical events for the low and high Reynolds number cases respectively. LESP is independent of motion kinematics for events 1 and 3 but increases with pitch rate for event 2 at low Reynolds number. Trends in LESP for the high Reynolds number simulations are similar to the trends observed for the NACA0012 airfoil's medium and high- K simulations where

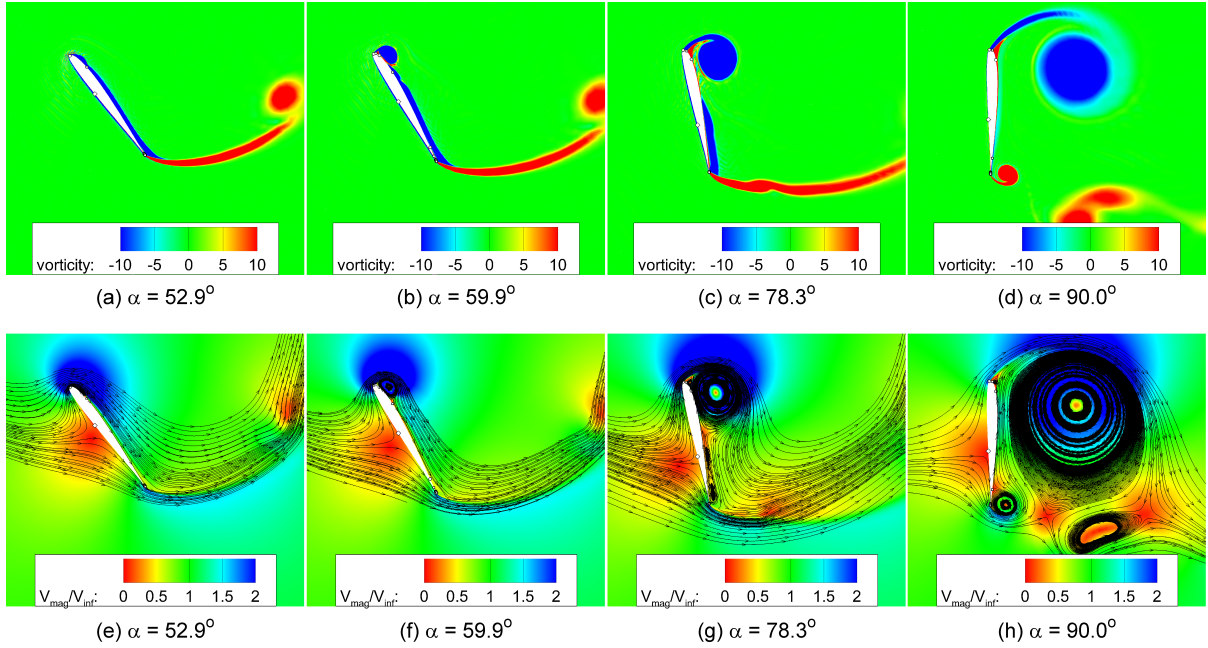


Figure 17: Vorticity (a – d) and velocity magnitude (e – h) contours for SD7003 unsteady simulations ($Re = 3 \times 10^6$, $K = 0.40$, 0° - 90° - 90° - 0° pitch up-hold-return).

event 1 is relatively independent of motion kinematics while events 2 and 3 increase with pitch rate. The reason for the tighter spread in LESP distributions for the low Reynolds number cases can be explained by revisiting the definition of LESP.

LESP is set to the A_0 value of the Fourier coefficient which is basically a measure of the suction/velocity at the leading-edge. On further observing Fig. 20(b), we see that at the point of LEV initiation, the majority of the flow dynamics are concentrated very close to the leading-edge. On the other hand, at a higher Reynolds number (Fig. 19(b)), the reversed flow region extends up to 17% of the chord. As a result, LESP fails to fully represent the suction characteristics beyond the vicinity of the leading edge which could cause the larger spread of data in Fig. 22.

Figures 23 and 24 show the variation of stagnation point with varying pitch rate and pivot location. There is no observable trend in stagnation point locations at the three events for the low Reynolds number cases. For the high Reynolds number cases, stagnation point location for event 1 has a tighter spread as compared to events 2 and 3.

IV. Conclusions

In this paper, numerical simulations were performed for the NACA0012 and SD7003 airfoils at low and high Reynolds numbers to study the variation of leading-edge suction in steady and unsteady motions. Vorticity and velocity magnitude contours were used to correlate the leading-edge suction data in order to gain a better understanding of the flow morphology with change in leading-edge suction. Steady results for the NACA0012 airfoil at a freestream Reynolds number of 3.0 million showed the the leading-edge suction increases with increasing angle of attack until steady stall after which there is a sharp drop in suction force. Next, the effect of variations in pitch rate on leading-edge suction was analyzed for the NACA0012 airfoil at $Re = 3 \times 10^6$ for three pitch rate regions: the low- K motions where only trailing-edge separation occurs, the medium- K motions where significant trailing-edge separation is followed by an LEV formation, and the high- K motions where there is minimal trailing-edge separation before LEV initiation.

Flowfield structures of the steady and unsteady low- K solutions compared well for a given separation location. However, lift force continued to increase beyond static stall for the unsteady case. The lift overshoot is attributed primarily to the boundary-layer convective lag. Beyond unsteady stall, steady and low- K aerodynamic coefficients are relatively similar.

For the LEV dominated motions, three critical events were defined and leading-edge suction at these points was studied. Flow contours showed that though leading-edge separation first occurs at event 1, the LEV does not start forming until event 2. Plots of LESP at the three events for varying pitch rates and pivot locations showed that while event 1 is independent of motion kinematics, the LESP for events 2 and 3 increases with increasing pitch rate. The observation was contradictory to results obtained by Ramesh et al. [49]. Further analysis focused on Reynolds number

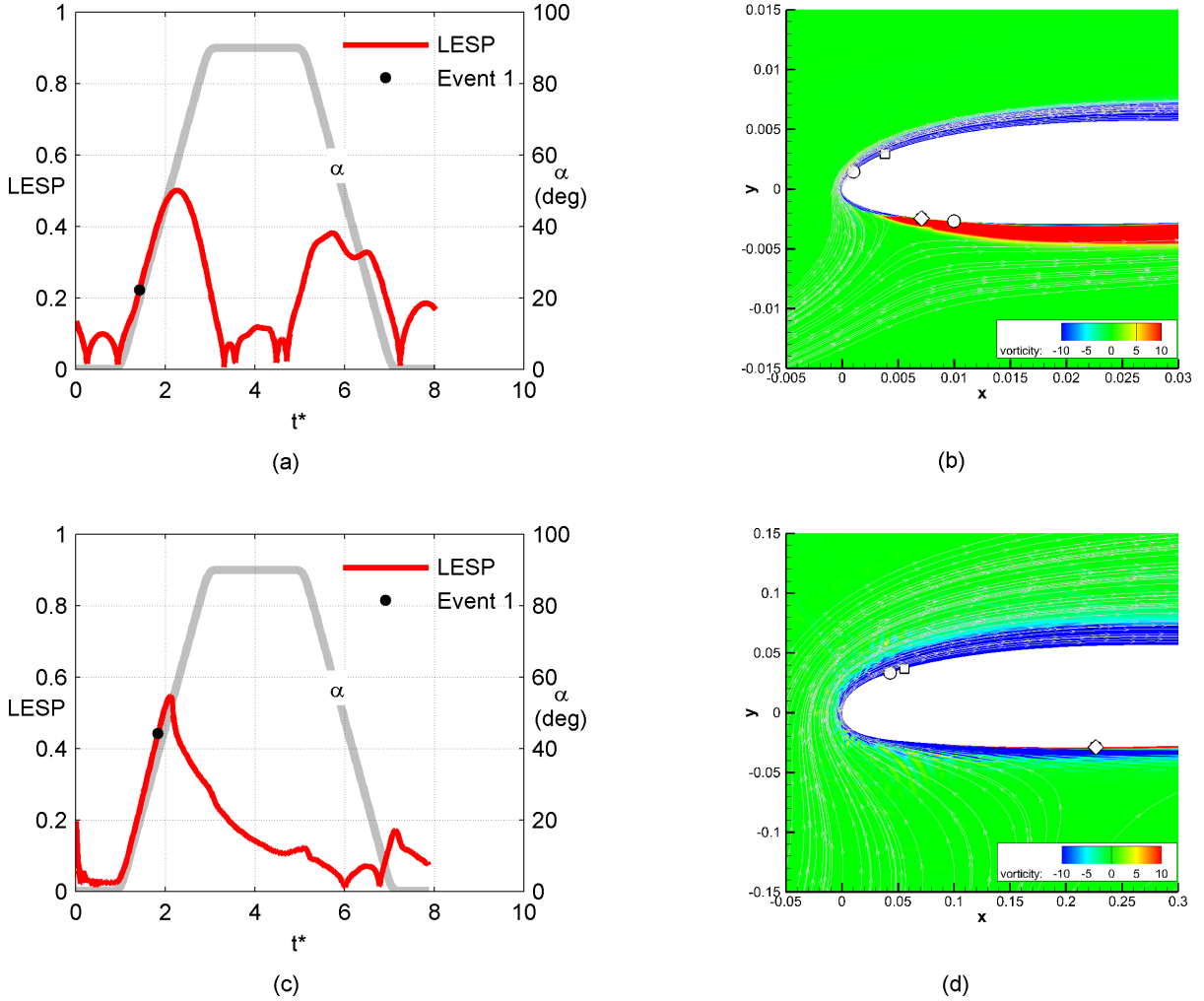


Figure 18: Event 1 comparison for low and high Reynolds numbers.

effects on leading-edge suction. The SD7003 airfoil was simulated for a range of pitch rates at $Re = 30,000$ and $Re = 3 \times 10^6$. Two main differences were observed that helped explain the reasons for the variations in leading-edge suction force at low and high Reynolds numbers. The first difference was that event 3 is the point of LEV initiation in the low Reynolds number cases as opposed to the high Reynolds number case where LEV initiation occurs at event 2. The second difference was seen when the LESP variation for a range of pitch rates and pivot locations was plotted. Events 1 and 3 in the low Reynolds number cases were found to be independent of motion kinematics while only event 1 showed relative independence to motion kinematics in the high Reynolds number cases. Further analysis of the flow contours showed that the separation region at the leading edge was spread across 17% of the chord for the high Reynolds number cases. On the contrary, in the low Reynolds number simulations, the separation region was restricted to a region very close to the leading edge (< 10%). The LESP parameter gives a good measure of the suction close to the leading-edge but fails to capture the effects aft of the leading-edge.

Finally, plots of stagnation point location with variations in pitch rate and pivot location showed no observable trend for the low Reynolds number cases but showed a tight spread for event 1 and increase with pitch rate for events 2 and 3 at high Reynolds number.

V. Acknowledgments

The authors wish to gratefully acknowledge the support of the U.S. Army Research Office through grant W911NF-13-1-0061, monitored formerly by Dr. Frederick Ferguson and currently by Dr. Matthew Munson.

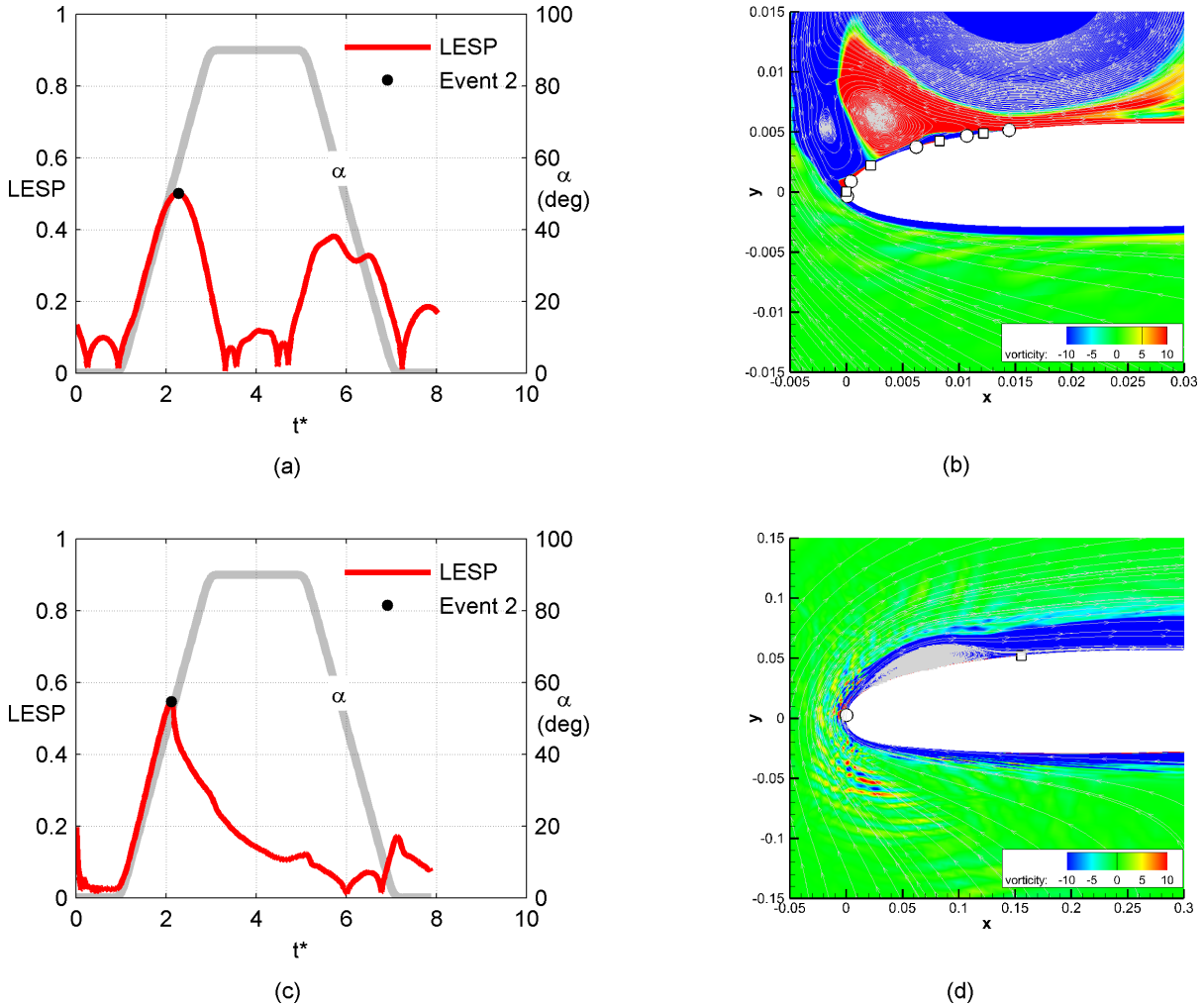


Figure 19: Event 2 comparison for low and high Reynolds numbers.

References

- [1] Corke, T. C. and Thomas, F. O., "Dynamic Stall in Pitching Airfoils: Aerodynamic Damping and Compressibility Effects," *Annual Review of Fluid Mechanics*, Vol. 47, 2015, pp. 479–505.
- [2] Huyer, S. A., Simms, D., and Robinson, M. C., "Unsteady aerodynamics associated with a horizontal-axis wind turbine," *AIAA Journal*, Vol. 34, No. 7, 1996, pp. 1410–1419.
- [3] Ellington, C. P., van den Berg, C., Willmott, A. P., and Thomas, A. L. R., "Leading-Edge Vortices in Insect Flight," *Nature*, Vol. 384, 1996, pp. 626–630.
- [4] Ellington, C., "The novel aerodynamics of insect flight: applications to micro-air vehicles," *Journal of Experimental Biology*, Vol. 202, No. 23, 1999, pp. 3439–3448.
- [5] Brown, C. E. and William H. Michael, J., "On Slender Delta Wings and Leading-Edge Separation," NACA TN 3430, 1955.
- [6] Young, J., Lai, J. C. S., and Platzer, M. F., "A review of progress and challenges in flapping foil power generation," *Progress in Aerospace Sciences*, Vol. 67, 2014, pp. 2 – 28.
- [7] Theodorsen, T., "General Theory of Aerodynamic Instability and the Mechanism of Flutter," NACA Rept. 496, 1935.
- [8] Wagner, H., "Über die Entstehung des dynamischen Auftriebes von Tragflügeln," *ZaMM*, Vol. 5, No. 1, 1925, pp. 17–35.
- [9] Crimi, P., "Dynamic Stall," AGARD-AG 172, 1973.
- [10] Carta, F., "An Analysis of the Stall Flutter Instability of Helicopter Rotor Blades," *Journal of the American Helicopter Society*, Vol. 12, 1967, pp. 1–18.
- [11] Carta, F., "Unsteady Normal Force on an Airfoil in a Periodically Stalled Inlet Flow," *Journal of Aircraft*, Vol. 4, No. 5, pp. 416–442.

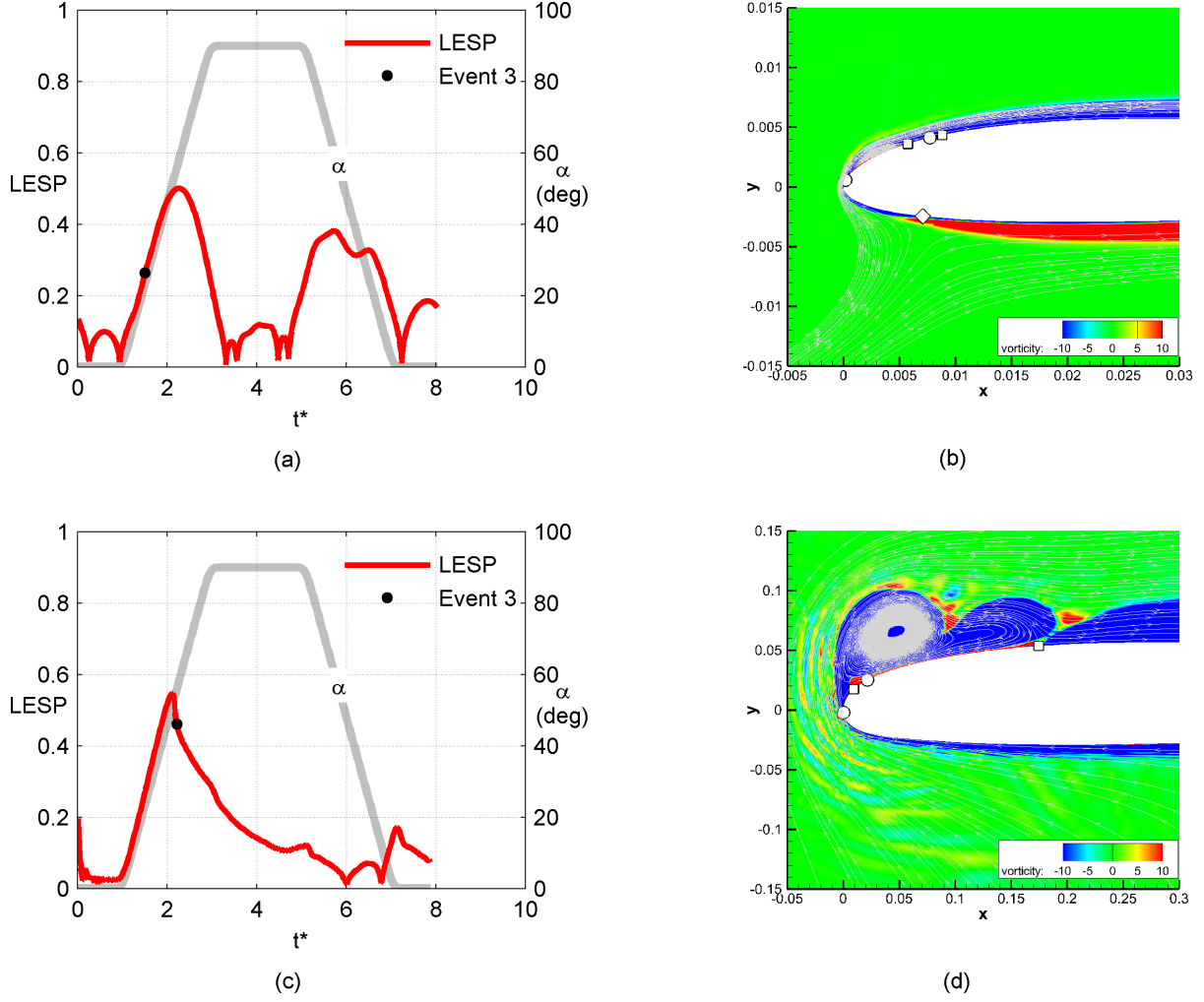


Figure 20: Event 3 comparison for low and high Reynolds numbers.

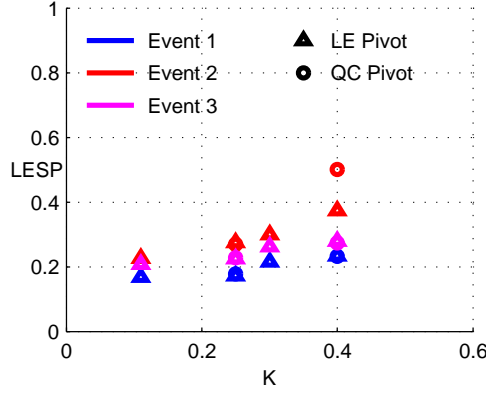


Figure 21: Variation of LESP with K for the three critical events at low Reynolds number.

- [12] Ericsson, L. E. and Reding, J. P., "Unsteady Airfoil Stall, Review and Extension," *Journal of Aircraft*, Vol. 8, No. 8, pp. 609–616.
- [13] McCroskey, W. J., Carr, L. W., and McAlister, K. W., "Dynamic stall experiments on oscillating airfoils," *AIAA Journal*, Vol. 14, No. 1, 1976, pp. 57–63.
- [14] McAlister, K. W., Carr, L. W., and McCroskey, W. J., "Dynamic Stall Experiments on the NACA0012 Airfoil," NASA TP

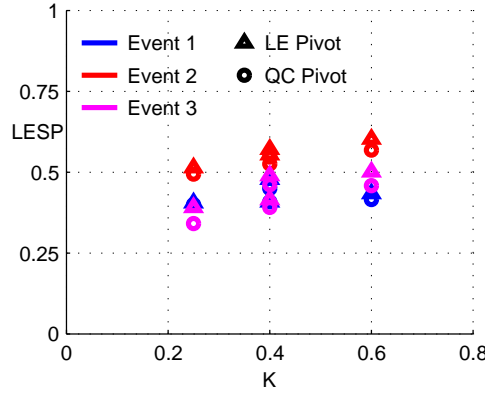


Figure 22: Variation of LESP with K for the three critical events at high Reynolds number.

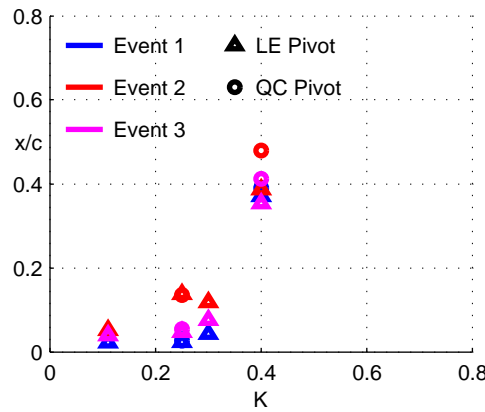


Figure 23: Variation of stagnation point with K for the three critical events at low Reynolds number.

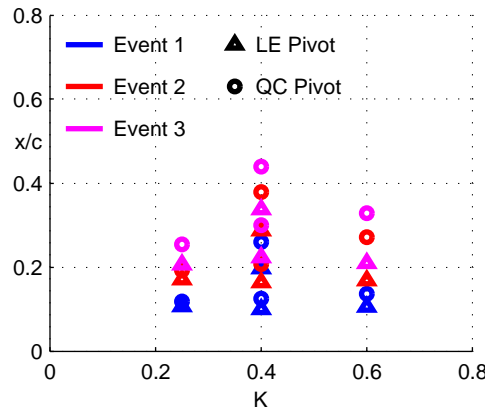


Figure 24: Variation of stagnation point with K for the three critical events at high Reynolds number.

1100, January 1978.

- [15] Carr, L. W., McAlister, K. W., and McCroskey, W. J., "Analysis of the Development of Dynamic Stall Based on Oscillating Airfoil Experiments," Nasa tn, January 1977.
- [16] McAlister, K. W. and Carr, L. W., "Water-Tunnel Experiments on an Oscillating Airfoil at $Re = 21,000$," NASA TM 78446, March 1978.
- [17] McCroskey, W., "Unsteady Airfoils," *Annual Review of Fluid Mechanics*, 1982, pp. 285–311.
- [18] McCroskey, W. J., "The Phenomenon of Dynamic Stall," NASA TM 81264, 1981.

- [19] McCroskey, W. J., McAlister, K. W., Carr, L. W., and Pucci, S. L., "An Experimental Study of Dynamic Stall on Advanced Airfoil Sections. Volume 1: Summary of the Experiment," NASA TM 84245, July 1982.
- [20] McAlister, K. W., Pucci, S. L., McCroskey, W. J., and Carr, L. W., "An Experimental Study of Dynamic Stall on Advanced Airfoil Sections. Volume 2: Pressure and Force Data," NASA TM 84245, September 1982.
- [21] Carr, L. W., McCroskey, W. J., McAlister, K. W., Pucci, S. L., and Lambert, O., "An Experimental Study of Dynamic Stall on Advanced Airfoil Sections. Volume 3: Hot-Wire and Hot-Film Measurements," NASA TM 84245, December 1982.
- [22] Visbal, M. and Shang, J., "Investigation of the Flow Structure Around a Rapidly Pitching Airfoil," *AIAA Journal*, Vol. 27, No. 8, 1989, pp. 1044–1051.
- [23] Ghosh Choudhuri, P. and Knight, D. D., "Effects of Compressibility, Pitch Rate, and Reynolds Number on Unsteady Incipient Leading-Edge Boundary Layer Separation Over a Pitching Airfoil," *Journal of Fluid Mechanics*, Vol. 308, 1996, pp. 195–217.
- [24] Ghosh Choudhuri, P., Knight, D., and Visbal, M. R., "Two-dimensional unsteady leading-edge separation on a pitching airfoil," *AIAA Journal*, Vol. 32, No. 4, 1994, pp. 673–681.
- [25] Akbari, M. H. and Price, S. J., "Simulation of Dynamic Stall for a NACA0012 airfoil using a Vortex Method," *Journal of Fluids and Structures*, Vol. 17, pp. 855–874.
- [26] Wernert, P., Geissler, W., Raffel, M., and Kompenhaus, J., "Experimental and Numerical Investigations of Dynamic Stall on a Pitching Airfoil," *AIAA Journal*, Vol. 34, No. 5, 1996, pp. 982–989.
- [27] Hill, J. L., Shaw, S. T., and Qin, N., "Investigation of Transition Modelling for a Aerofoil Dynamic Stall," Tech. rep., 2004.
- [28] Geissler, W. and Haselmeyer, H., "Investigation of Dynamic Stall Onset," *Aerospace Science and Technology*, Vol. 10, pp. 590–600.
- [29] Spentzos, A., Barakos, G., Badcock, K., Richards, B., Wernert, P., Schreck, S., and Raffel, M., "CFD Investigation of 2D and 3D Dynamic Stall," Proceedings of the ahs 4the decennial specialist's conference on aeromechanics, san francisco, california, usa, January 2004.
- [30] Eldredge, J. D. and Wang, C., "High-fidelity simulations and low-order modeling of a rapidly pitching plate." AIAA paper 2010-4281, 2010, In review for publication in *Journal of Theoretical and Computational Fluid Dynamics*.
- [31] Eldredge, J. D., Wang, C. J., and Ol, M. V., "A computational study of a canonical pitch-up, pitch-down wing maneuver," AIAA Paper 2009-3687, 2009.
- [32] "Experiments and computations on abstractions of perching." Tech. rep.
- [33] Ol, M., Bernal, L., Kang, C., and Shyy, W., "Shallow and deep dynamic stall for flapping low Reynolds number airfoils," *Experiments in fluids*, Vol. 46, No. 5, 2009, pp. 883–901.
- [34] Gormont, R. E., "A Mathematical Model of Unsteady Aerodynamics and Radial Flow for Application to Helicopter Rotors," Army air mobility research and development laboratory tr, May 1973.
- [35] Dat, R., Tran, C. T., and Petot, D., "Modele Phenomenologique de Decrochage Dynamique sur Profil de Pale d'Helicoptere," ONERA TP 1979, 1979.
- [36] Leishman, J. and Beddoes, T., "A Semi-Empirical Model for Dynamic Stall," *Journal of the American Helicopter Society*, Vol. 34, 1989, pp. 3–17.
- [37] Katz, J., "Discrete vortex method for the non-steady separated flow over an airfoil," *Journal of Fluid Mechanics*, Vol. 102, 1981, pp. 315–328.
- [38] Larsen, J. W., Nielsen, S. R. K., and Krenk, S., "Dynamic Stall Model for Wind Turbine Airfoils," *Journal of Fluids and Structures*, Vol. 23, No. 7, 2007, pp. 959–982.
- [39] Sheng, W., Galbraith, R. A. M., and Coton, F. N., "A New Stall-Onset Criterion for Low Speed Dynamic-Stall," *Journal of Solar Energy Engineering*, Vol. 128, No. 4, 2006, pp. 461–471.
- [40] Sheng, W., Galbraith, R. A. M., and Coton, F. N., "A Modified Dynamic Stall Model for Low Mach Numbers," *Journal of Solar Energy Engineering*, Vol. 130, No. 3, 2008, pp. 31013–31023.
- [41] Yan, Z., Taha, H. E., and Hajj, M. R., "Geometrically-Exact Unsteady Model for Airfoils Undergoing Large Amplitude Maneuvers," *Aerospace Science and Technology*.
- [42] Evans, W. T. and Mort, K. W., "Analysis of Computed Flow Parameters for a set of Sudden Stalls in Low Speed Two-Dimensional Flow," NACA Report TN D-85, 1959.
- [43] T.S.Beddoes, "Onset of Leading Edge Separation Effects under Dynamic Conditions and Low Mach Number," 34th Annual forum of the American Helicopter Society, 1978.
- [44] Jones, K. D. and Platzer, M. F., "A fast method for the prediction of dynamic stall onset on turbomachinery blades," ASME Paper 97-GT-101, 1997.
- [45] Chandrasekhara, M. S., Ahmed, S., and Carr, L. W., "Schlieren studies of compressibility effects on dynamic stall of transiently pitching airfoils," *Journal of Aircraft*, Vol. 30, No. 2, March–April 1993, pp. 213–220.

- [46] Ekaterinaris, J. A. and Platzer, M. F., "Computational prediction of airfoil dynamic stall," *Progress in Aerospace Sciences*, Vol. 33, No. 11–12, 1998, pp. 759–846.
- [47] Jones, K. and Platzer, M., "On the prediction of dynamic stall onset on airfoils in low speed flow," *Proceedings of the 8th International Symposium on Unsteady Aerodynamics and Aeroelasticity of Turbomachines*, 1998, pp. 797–812.
- [48] Ramesh, K., Gopalarathnam, A., Edwards, J. R., Ol, M. V., and Granlund, K., "An Unsteady Airfoil Theory Applied to Pitching Motions Validated against Experiment and Computation," *Theoretical and Computational Fluid Dynamics*, Vol. ISSN 0935-4964, January 2013.
- [49] Ramesh, K., Gopalarathnam, A., Granlund, K., Ol, M. V., and Edwards, J. R., "Discrete-vortex method with novel shedding criterion for unsteady airfoil flows with intermittent leading-edge vortex shedding," *Journal of Fluid Mechanics*, Vol. 751, July 2014, pp. 500–538.
- [50] Narsipur, S., Gopalarathnam, A., and Edwards, J. R., "A Time-Lag Approach for Prediction of Trailing-Edge Separation in Unsteady Flow," Proceedings of the AIAA Aviation Congerence, Atlanta, GA 2014-2701, June 2014.
- [51] Cassidy, D. A., Edwards, J. R., and Tian, M., "An Investigation of Interface-Sharpening Schemes for Multiphase Mixture Flows," *Journal of Computational Physics*, Vol. 228, No. 16, 2009, pp. 5628–5649.
- [52] Spalart, P. R. and Allmaras, S. R., "A One-Equation Turbulence Model for Aerodynamic Flows," AIAA Paper 92-0439, 1992.
- [53] Edwards, J. R. and Chandra, S., "Comparison of Eddy Viscosity - Transport Turbulence Models for Three-Dimensional, Shock-Separated Flowfields," *AIAA Journal*, Vol. 34, No. 4, 1996, pp. 756–763.
- [54] Eldredge, J. and Wang, C., "Improved low-order modeling of a pitching and perching plate," AIAA Paper 2011-3579, 2011.
- [55] Ericsson, L. E. and Reding, J. P., "Fluid Mechanics of Dynamic Stall Part I. Unsteady Flow Concepts," *Journal of Fluids and Structures*, Vol. 2, No. 1, 1988, pp. 1–33.